JACS Au
AN OPEN ACCESS JOURNAL OF THE AMERICAN CHEMICAL SOCIETY

pubs.acs.org/jacsau
Article

Formation of a Pd_{16} Molecular Basket Architecture of Reduced Symmetry and Angular Deviation in a Fluorenone Scaffold to Govern the Host–Guest Chemistry of Pd_6 Trifacial Tubes

Medha Aggarwal, Ranit Banerjee, Neal Hickey, and Partha Sarathi Mukherjee*

Cite This: *JACS Au* 2025, 5, 2368–2378
Read Online

ACCESS | Metrics & More | Article Recommendations | Supporting Information

ABSTRACT: The employment of flexible ligands with significant conformational freedom in coordination-driven self-assembly enables the formation of unique and intricate structures. In this study, the self-assembly of such a fluorenone-appended ligand (**L1**) with a sterically demanding acceptor, [Pd(tmed)$(ONO_2)_2$] (**M1**), generated a new and unique molecular basket architecture, $(\mathbf{M1})_{16}(\mathbf{L1})_8$ (**B**), featuring a large hollow cavity. **B** possesses an unusual twisted architecture of low symmetry, consisting of 16 Pd(II) centers arranged as four tetrahedra connected by eight flexible ligands, representing a structurally complex system reminiscent of biological architectures. Designing such entropically disfavored, large architectures of reduced symmetry is challenging but desirable, since they can act as ideal models to study complicated natural systems. The host–guest property of supramolecular hosts is governed by the confined cavities and noncovalent interactions, which are dictated by the angular disposition of ligand coordination sites. To explore this, the fluorenone scaffold was used to synthesize two other tetradentate ligands (**L2** and **L3**) that differed in the spatial distributions of their coordination vectors. The self-assembly of these ligands with [Pd(en)$(ONO_2)_2$] (**M2**) resulted in the formation of water-soluble $(\mathbf{M2})_6(\mathbf{L1/L2/L3})_3$ trifacial tubes of different geometries with varying internal cavity dimensions. These angular variations further altered the orientation of the fluorenone carbonyl groups within the cavities, thereby modulating their guest binding abilities and highlighting the importance of tailoring supramolecular hosts for specific guest binding.

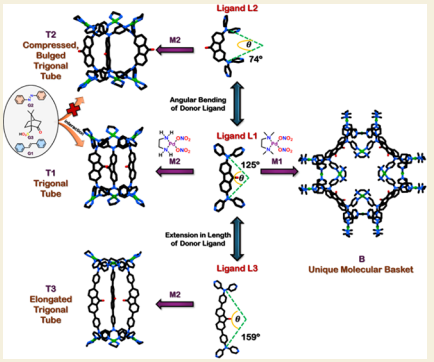

KEYWORDS: *self-assembly, coordination chemistry, cage compounds, unique supramolecular architecture, host–guest chemistry*

INTRODUCTION

Coordination-driven self-assembly is a powerful tool for designing metal–organic cages with appealing properties.[1−10] Large and complicated architectures can be easily synthesized using this strategy without involving any synthetic complexities, unlike other supramolecular techniques.[11−14] However, most coordination cages reported to date possess symmetric, regular polyhedral geometries.[15] This is mainly due to nature's preference for higher-order architectures and also the fact that asymmetric building units often fail to assemble into discrete stable cages, rendering the synthesis of structures of lower symmetry challenging. However, there is a rising urge among supramolecular chemists to synthesize desymmetrized cages since they can act as ideal models for studying various complex biological processes.[16,17] To that end, the utilization of donor ligands with moderate pliability and acceptors with steric requirements holds good promise.[18−20]

Discrete supramolecular cages can bind guests via various noncovalent interactions, identical to biological systems.[21−31] For instance, enzymes can selectively bind substrates, and their catalytic activity significantly depends on the geometries and functionalities of their active sites as well as the steric environment around them. Similarly, artificial systems like discrete metal–organic cages, depending on the design of their internal pockets, can mimic these conducive conditions, making them suitable for applications such as catalysis,[32−36] molecular separations by selective encapsulation,[37−40] and stabilization of reactive molecules.[41−43] Two factors play decisive roles in determining the nature of the internal cavities of such hosts. First, the core functionalities dictate the noncovalent interactions offered to the incoming guests.[44−47] Second, the angles between the planes of the ring containing the donor heteroatoms and the plane of the central ring of the ligands, or in other words, the relative spatial disposition of the coordinating atoms of ligands, can control the dimensions of the internal pockets.[48] In the past few years, some groups have shown that variation in the dihedral angles of ditopic ligands can influence the nature of the self-assembled product

Received: April 3, 2025
Revised: April 29, 2025
Accepted: April 29, 2025
Published: May 9, 2025

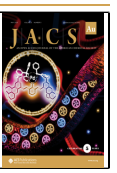

Scheme 1. Schematic Representation of the Formation of a Unique Pd_{16} Molecular Basket Architecture (B) via Self-Assembly of Ligand L1 with *cis*-[(tmed)Pd(ONO_2)$_2$] (M1)

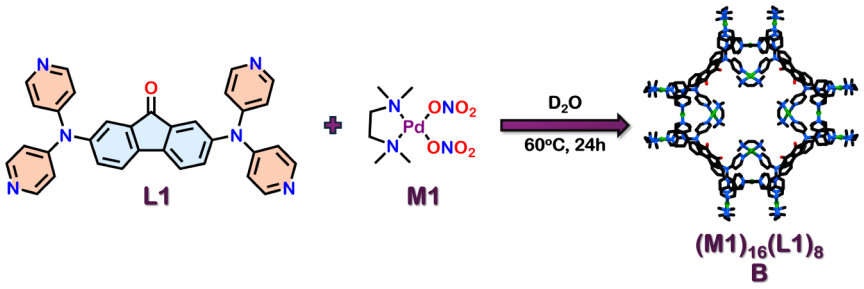

obtained with naked Pd(II) ions.[49−53] Recently, the effect of the dihedral angles of tritopic ligands on the nature of final assemblies obtained with a 90° *cis*-blocked Pd(II) metal acceptor was demonstrated.[54] However, the effect of such angular modulation of tetratopic ligands on the structure of final host assemblies and the variation in their guest-stabilizing abilities due to such modification is still underexplored. In this regard, molecular barrels generated from tetratopic ligands and 90° metal acceptors are helpful; first, since it is easier to install functionalities symmetrically within tetradentate ligands with varying angular dispositions of the heteroatoms, and second, due to the inherent ability of such hosts to stabilize a wide range of guest molecules.[55]

Herein, we report the formation of a unique Pd_{16} molecular basket architecture (**B**) via the self-assembly of ligand **L1** and *cis*-[(tmed)Pd(NO_3)$_2$] (**M1**) [tmed = *N*,*N*′,*N*′-tetramethylethane-1,2-diamine] (Scheme 1). Generally, the combination of tetratopic donors and 90° Pd(II) acceptors results in the formation of molecular barrels or higher-order symmetric Johnson polyhedra.[15,55] Interestingly, the SC-XRD structure of **B** resembles neither. Rather, the donor ligands are heavily intertwined and connected to four sets of Pd_4 tetrahedra, giving an unprecedented hollow, basket-shaped structure. This appears to be driven mainly by the flexibility of **L1**. A simple coordination-driven self-assembly reaction of such building units enabled the fabrication of a twisted, complex, and entropically disfavored architecture closely resembling biological systems, which is otherwise cumbersome or impossible using covalent bond-formation techniques.

Further, two other fluorenone-based tetradentate ligands, **L2** and **L3**, were synthesized. The ligands differed in their relative angular orientation of the donor atoms with respect to the fluorenone core (**L1** and **L2**) or lengths from the central fluorenone core (**L1** and **L3**). Interestingly, the self-assembly of the three different ligands with the Pd(II) acceptor, *cis*-[Pd(en)(NO_3)$_2$] (**M2**), resulted in the formation of (**M2**)$_6$(**L1**/**L2**/**L3**)$_3$ trifacial tubes of varying dimensions in aqueous media [en = ethane-1,2-diamine] (Scheme 2). An exciting aspect of these tubes was that the orientation of the fluorenone carbonyl groups of the hosts with respect to the cavity of the tubes, was governed by the angular deviation in the respective ligands. In **T1**, all the fluorenone oxygen atoms were oriented into the cavities of the respective tubes. On the other hand, in **T2**, the fluorenone oxygens resided outside the cavity. This orientation of the carbonyl oxygens greatly influenced their ability to stabilize guests. While **T1** could encapsulate guests like **G1** (E-stilbene)[56] or **G2** (azobenzene) and even water-soluble guests like **G3** (camphor sulfonic acid), **T2** did not encapsulate such guest molecules (Scheme 4).

Scheme 2. Schematic Representation of the Synthesis of Trifacial Tubes, T*n* (*n* = 1−3) Possessing Different Geometries and Cavity Sizes Obtained via Modification of Ligand L1 by Angular Bending of Donor Ligand to Form L2 and Extension of Donor Length to Form the Ligand L3[a]

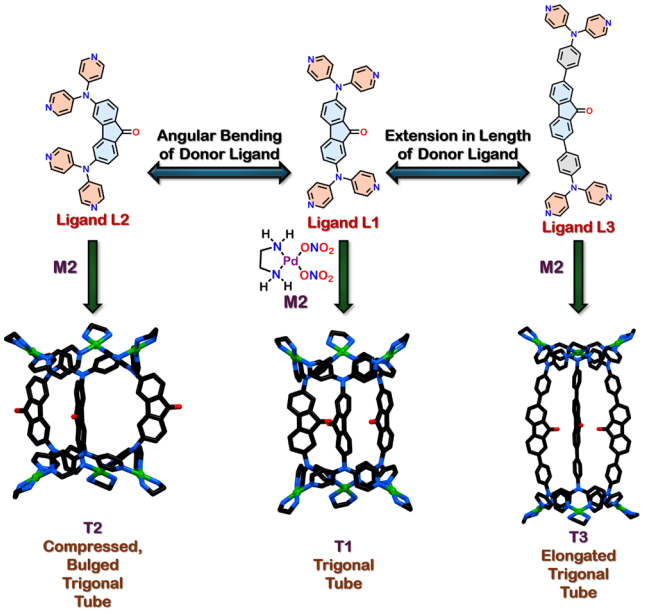

[a]The self-assembly of **L1**/**L2**/**L3** with **M2** leads to the formation of trifacial tubes **T1**/**T2**/**T3** having a similar (**M2**)$_6$(**L1**/**L2**/**L3**)$_3$ composition.

Stabilization of the guests within the cavity of **T1** was driven by the H-bonding interactions between the carbonyl oxygen of fluorenone with guest protons and cavity size compatibility with such guests, which was not possible in **T2** due to the outward orientation of fluorenone carbonyl groups and shorter cavity length. Thus, here we demonstrate the role of functionalities and their orientations with respect to the confined pockets in determining their host−guest properties.

METHODS

All of the chemicals and solvents were purchased from different commercially available sources and used directly without further purification. NMR studies were performed on Bruker 400 MHz and 500 MHz spectrometers. The chemical shifts (δ) in the ^{1}H NMR spectra were reported in ppm relative to the tetramethylsilane (TMS), which was used as an internal standard (δ = 0.00 ppm) for $CDCl_3$ or the resonance of the proton resulting from partial deuteration of the NMR solvent: D_2O (δ = 4.79 ppm). Electrospray ionization mass spectra were recorded using an Agilent 6538 Ultra-High Definition

https://doi.org/10.1021/jacsau.5c00390
JACS Au 2025, 5, 2368−2378

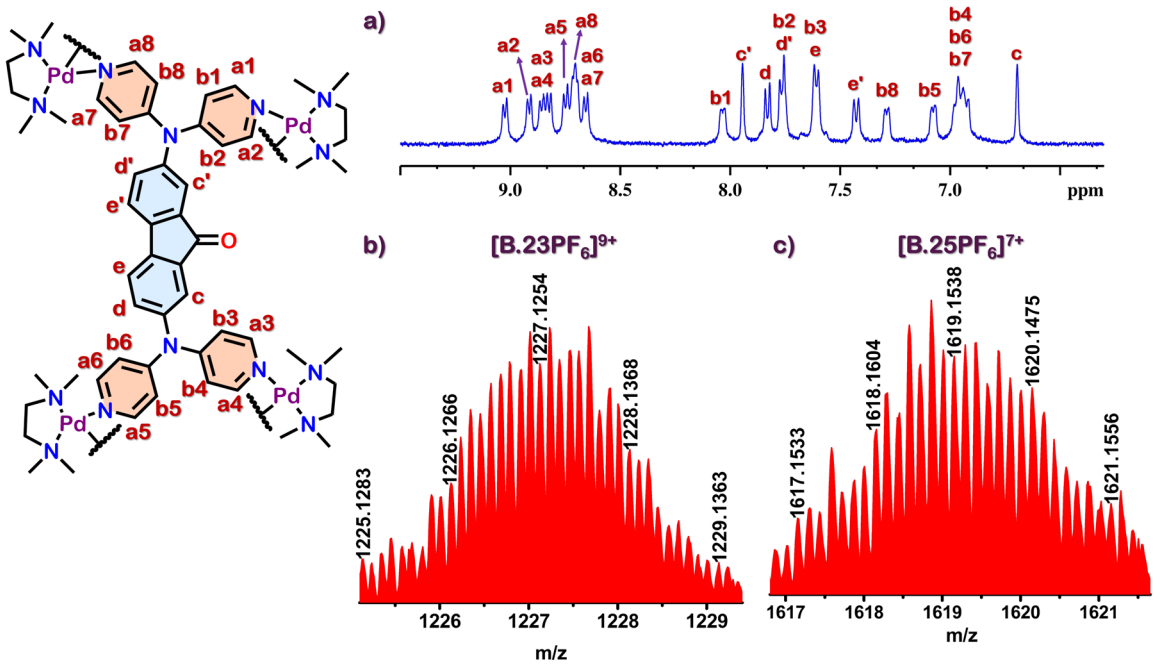

Figure 1. (a) ^{1}H NMR spectrum of **B** recorded in D_2O. Isotopic patterns obtained in ESI-MS of the PF_6^- analogue, recorded in CH_3CN corresponding to the charged fragments: (b) $[\mathbf{B}{\cdot}23PF_6]^{9+}$ and (c) $[\mathbf{B}{\cdot}25PF_6]^{7+}$.

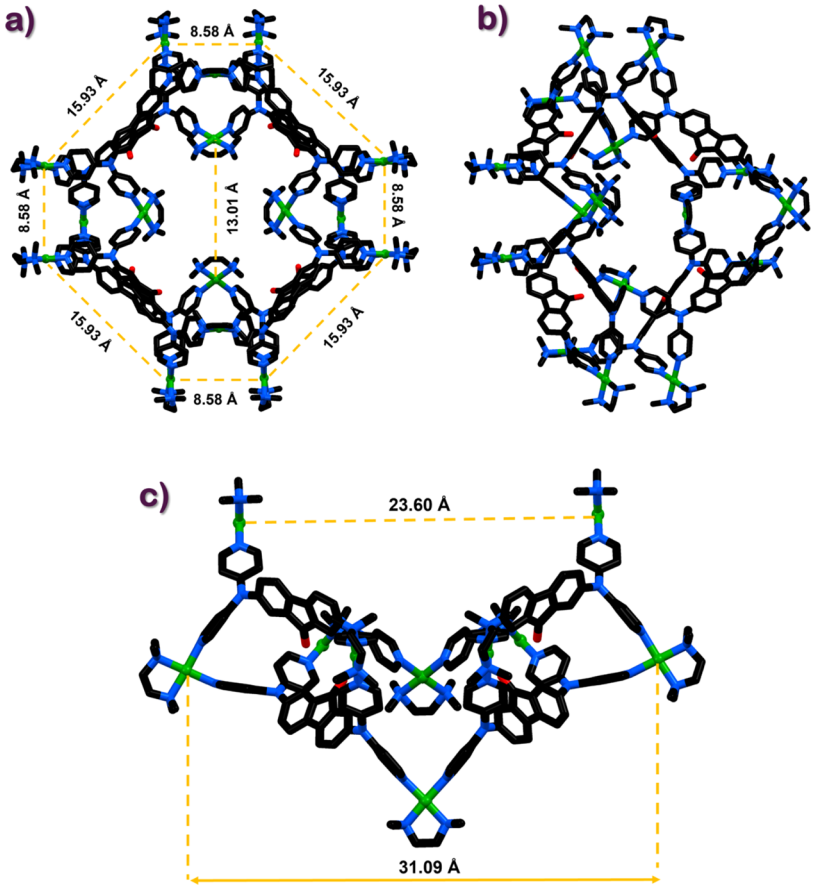

Figure 2. SC-XRD structure of **B**: (a) top view, (b) diagonal view, and (c) side view. Color codes: carbon (black), nitrogen (blue), oxygen (red), and palladium (green). Solvent molecules, counter-anions, and H atoms are omitted for clarity.

(UHD) Accurate Mass Q-TOF spectrometer, along with the use of standard spectroscopic-grade solvents.

Single crystals were obtained by the diffusion of acetone into aqueous solutions of **B** or diffusion of 1,4-dioxane into the DMSO solution of **T3**. Single-crystal X-ray diffraction data of the crystals

https://doi.org/10.1021/jacsau.5c00390
JACS Au 2025, 5, 2368−2378

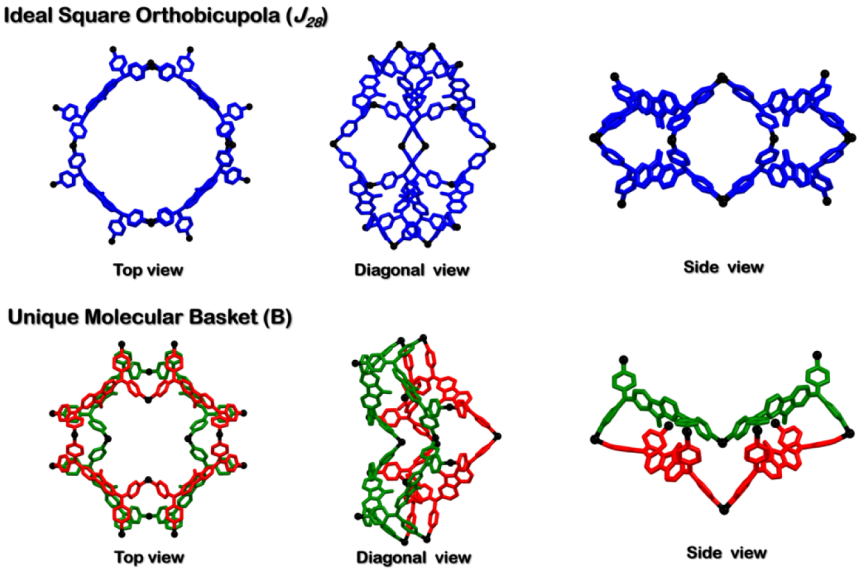

Figure 3. Comparison of the basket architecture (**B**) with an ideal square orthobicupola architecture. Color codes: For ideal orthobicupola: ligands (blue), Pd (black); for basket architecture: ligands (red and green), Pd (black). H atoms and the tetramethylethylenediamine caps of **M1** are omitted for clarity.

obtained were collected with a monochromatic wavelength of 0.7000 Å at the XRD1 beamline of the Elettra synchrotron, Trieste (Italy), employing the rotating-crystal method and a Dectris Pilatus 2M area detector (details provided in the Supporting Information).

DFT optimizations of all the assemblies **T1**, **T2**, and **T3** were carried out using the Gaussian 09 package. The single-point energies of **T1**, **T2**, and **T3** were calculated using the hybrid B3LYP functional with a mixed basis set of LanL2DZ (for Pd atom) and 6-31G(d) (for C, H, N, and O atoms).

The geometries of $(\mathbf{G3})_2$**@T1** and $(\mathbf{G3})_2$**@T2** were optimized using the PM6 semiempirical method using the Gaussian 09 package.

RESULTS AND DISCUSSION

Synthesis of a New and Unique Pd_{16} Molecular Basket Architecture of Reduced Symmetry

The flexible ligand **L1** was synthesized via an Ullmann coupling reaction of 2,7-bis(dibromo-9*H*-fluoren-9-one) with 4,4'-dipyridylamine.[56] The in situ reaction of **L1** with the acceptor *cis*-[(tmed)Pd$(NO_3)_2$] (**M1**) in a 1:2 molar ratio at 60 °C in D_2O for 24 h resulted in a clear amber-colored solution, indicating the formation of a self-assembled product, **B** (Schemes 1 and S5). Multiple sharp and distinct peaks were observed in the aromatic region of the ^{1}H NMR spectrum of self-assembled product **B** (Figures 1a and S6), in sharp contrast to the five peaks in the aromatic region of the building block (**L1**). Multiple splittings of proton peaks in ^{1}H NMR may originate from multiple assemblies. However, the single diffusion band in ^{1}H-DOSY NMR confirmed the presence of only one species (D = 8.91 × 10^{-11} m^2/s) with a large hydrodynamic radius (r = 27.8 Å) (Figure S7). All the peaks in the ^{1}H NMR spectrum were assigned with the help of ^{1}H−^{1}H COSY NMR (Figure S8). Eight sets of α and β pyridyl protons were observed, indicating the formation of a molecular architecture (**B**) in which the ligands (**L1**) assume several different orientations. To determine the actual composition of **B**, it was subjected to ESI-MS analyses after converting the water-soluble NO_3^- salt to its acetonitrile-soluble PF_6^- analogue by treating it with excess KPF_6 for easier ionization under ESI-MS conditions. Several peaks and isotopic distributions were obtained in the ESI-MS at m/z = 1913.1742, 1619.1538, 1398.6333, 1227.1254, 1089.9237, 977.6564, and 884.1113, corresponding to the charged fragments $[\mathbf{B}\cdot26PF_6]^{6+}$, $[\mathbf{B}\cdot25PF_6]^{7+}$, $[\mathbf{B}\cdot24PF_6]^{8+}$, $[\mathbf{B}\cdot23PF_6]^{9+}$, $[\mathbf{B}\cdot22PF_6]^{10+}$, $[\mathbf{B}\cdot21PF_6]^{11+}$, and $[\mathbf{B}\cdot21PF_6]^{12+}$. These matched the theoretically calculated isotopic patterns, unambiguously confirming the composition of $(\mathbf{M1})_{16}(\mathbf{L1})_8$ (Figures 1b,c, S9, and S10).

Single crystals of **B** suitable for X-ray diffraction could be obtained by the slow diffusion of acetone vapors into a concentrated aqueous solution of the reaction mixture. **B** crystallizes in the tetragonal space group $I\bar{4}m2$. The SC-XRD structure of **B** displays a unique $(\mathbf{M1})_{16}(\mathbf{L1})_8$ hollow basket-like geometry, wherein the 16 Pd(II) acceptors are arranged as four approximate tetrahedra at the four corners, conjoined by the eight intertwined flexible ligands (**L1**) (Figures 2, S1d, and S4). There are several other ways of describing this unusual asymmetric architecture, **B**. In an ideal square orthobicupola architecture, the ligands (**L1**) occupy all 8 square faces of a Johnson Polyhedron (J_{28}), and the 16 metal acceptors are at the vertices.[57,58] Here, in contrast to that, four of the Pd(II) ions are displaced from their original vertex positions and are pushed into the center of the polyhedron, compelling a few of the ligands to twist in order to adhere to the coordination requirements, thereby desymmetrizing the higher-order structure (Figure 3). In terms of the arrangement of the 16 metal acceptors (**M1**), it somewhat resembles a square gyrobicupola, Johnson Polyhedron (J_{29}), with four Pd(II) ions displaced from their ideal vertex positions (Figure S5).

The structure of **B** can also be described as comprising two sets of $(\mathbf{M1})_4(\mathbf{L1})_4$ macrocycles (marked in red and green, respectively, in Figure 3) sitting on top of one another without interlocking on an octagonal base, wherein 8 Pd(II) ions complete the coordination of uncoordinated heteroatoms of **L1** in these two macrocyclic subunits (Figure 3). So, the inherent flexibility of the ligand enables twisting or desymmetrization of a symmetric Johnson polyhedron (J_{28}) structure, but at the same time, the restricted pliability of the building units and the steric effect of methyl groups adhered to the acceptors prevent interlocking to form a knot-like

https://doi.org/10.1021/jacsau.5c00390
JACS Au 2025, 5, 2368−2378

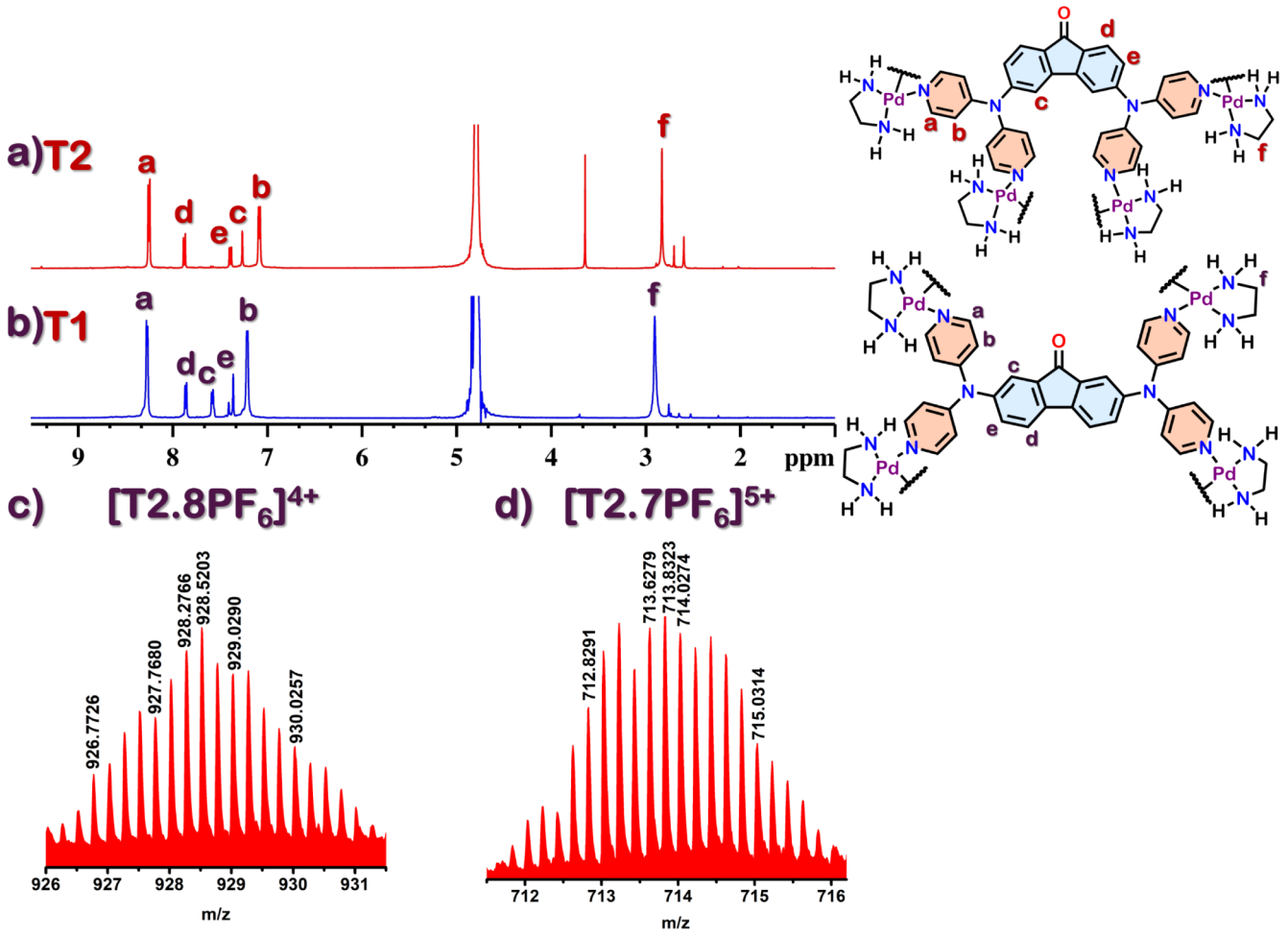

Figure 4. Stacked ^{1}H NMR spectra of (a) **T2** and (b) **T1** recorded in D_2O. Isotopic patterns obtained in ESI-MS of the PF_6^- analogue, recorded in CH_3CN corresponding to the charged fragments: (c) $[\mathbf{T2}{\cdot}8PF_6]^{4+}$ and (d) $[\mathbf{T2}{\cdot}7PF_6]^{5+}$.

structure. The ^{1}H NMR also corroborates this twisted architecture. In an ideal square orthobicupola architecture, the α- and β-pyridyl protons are expected to split into four sets due to two different chemical environments and inward and outward orientations of the pyridyl rings with respect to the cavity. On the other hand, the ^{1}H NMR spectrum of **B** in aqueous solution displays an 8-fold splitting of the pyridyl protons due to the additional desymmetrization, indicating that the asymmetry induced is maintained even in the solution state (Figure 1a). Fabrication of such higher-order desymmetrized architectures is challenging and has not been reported earlier to the best of our knowledge.

Synthesis of Trifacial Tubes of Different Shapes and Geometries via Angular Modulation

Although the inherent twisting ability of our building ligand (**L1**) and the steric effects incorporated by the tetramethylated acceptor (**M1**) enabled the formation of an aesthetically pleasing Pd_{16} molecular basket (**B**), it lacked a suitable confined cavity for stabilizing guest molecules (Figure S34). Contradictorily, when *cis*-$[Pd(en)(ONO_2)_2]$ (**M2**) is self-assembled with the same ligand (**L1**), a $(\mathbf{M2})_6(\mathbf{L1})_3$ trifacial tube (**T1**) is generated in aqueous solution, which was unambiguously confirmed from the SC-XRD structure in our recent report.[56] Further, we wanted to explore what effect the angular modulation of the building donors has on the final architectures and their host−guest chemistry. The angles can be modulated by altering the position of dipyridylamine binding sites to the fluorenone core. To this end, the ligand **L2** [3,6-bis(di(pyridin-4-yl)amino)-9*H*-fluoren-9-one] was synthesized via a copper-catalyzed Ullmann coupling reaction and was fully characterized using NMR and mass analyses (Scheme S1, Figures S11−S13).[56,59] Subsequently, the self-assembly of **L2** with **M2** was carried out in a 1:2 molar ratio at 60 °C in D_2O for 12 h, which resulted in a clear lime-colored solution (Schemes 2 and S7). An unsplit ^{1}H NMR pattern was observed for **T2**, like that of **T1**, indicating the formation of a simple molecular architecture (Figures 4a and S19). ^{1}H DOSY (Figure S20) further confirmed the formation of a single self-assembled product (diffusion coefficient, $D = 1.78 \times 10^{-10}$ m^2/s; hydrodynamic radius, r = 13.8 Å). The ESI-MS analyses of the corresponding PF_6^- analogue of **T2** confirmed its composition to be $(\mathbf{M2})_6(\mathbf{L2})_3$, akin to **T1**. Peaks and isotopic patterns were observed in ESI-MS at m/z = 1286.3477, 928.5203, and 713.8323, corresponding to the charged fragments $[\mathbf{T2}{\cdot}9PF_6]^{3+}$, $[\mathbf{T2}{\cdot}8PF_6]^{4+}$, and $[\mathbf{T2}{\cdot}7PF_6]^{5+}$, respectively, matching with the theoretical isotopic patterns (Figures 4c,d, S21, and S22).

Although the composition of **T2** is the same as that of **T1**, its geometry is expected to be different from that of **T1**. Despite several attempts, we could not obtain single crystals of **T2** that were suitable for X-ray diffraction. Thus, the geometry was optimized by using the density functional theory (DFT)

https://doi.org/10.1021/jacsau.5c00390
JACS Au 2025, 5, 2368−2378

method (Figure 5). The nonsolvated radius of the DFT-optimized structure (r = 13.1 Å, Figure S56, Table S5, and Section S8) corroborated quite well with the hydrodynamic radius obtained from DOSY (Figure S20, Table S5, and Section S8), confirming it to be the geometry of **T2**. Due to the vast angular differences in **L1** and **L2** (angle subtended by the dipyridyl amine units to the central fluorenone core: **L1** = ca. 125°; **L2** = ca. 74°), the carbonyl groups of fluorenone building units in **T2** can no longer remain directed toward the cavity of the tube (Figure 5).

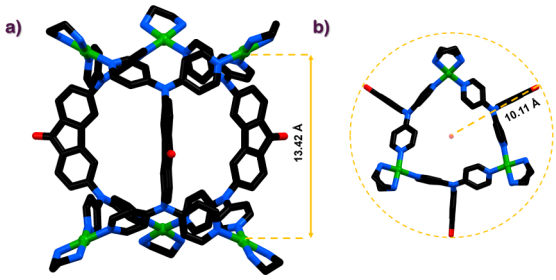

Figure 5. DFT optimized structure of **T2**: (a) side view and (b) top view. Color codes: carbon (black), nitrogen (blue), oxygen (red), and palladium (green). Hydrogen atoms are omitted for clarity.

The next amendment to the building units was done via the elongation of **L1** by two phenyl rings, which increased the angle subtended by the dipyridyl amine units to the fluorenone core of the ligand (**L3**) to ca. 159°. The ligand **L3** was synthesized in three steps (Schemes S2–S4, Figures S14–S18), and the reaction of **L3** with *cis*-blocked **M2** in a 1:2 molar ratio at 60 °C in DMSO for 12 h resulted in a clear orange solution (Scheme S8). The solution was centrifuged, and the DMSO solution was added to excess ethyl acetate (12 mL) to afford an orange precipitate, **T3**. The precipitate was thoroughly washed with acetone and dried in a vacuum. The precipitate was sparingly water-soluble upon heating, resulting in a very broad ^{1}H NMR spectrum. However, we obtained single crystals of the self-assembled product **T3** by the slow diffusion of 1,4-dioxane into the concentrated DMSO solution of **T3**. The SC-XRD structure confirms that **T3** has a trifacial $(\mathbf{M2})_6(\mathbf{L3})_3$ tube structure. **T3** crystallized in the hexagonal *P6/m* space group, with the 6 Pd(II) ions occupying the vertices of an equilateral prism defined by Pd···Pd distances of 10.962 Å (triangular faces) and 23.246 Å (prism length). The structure is analogous to that previously reported for **T1** (Figure 6).[56] Further details of the structure of **T3** are reported in Section S4 and Table S1.

The crystals of trifacial tube **T3** were sparingly soluble in aqueous media, and the ^{1}H NMR spectrum was recorded in D_2O. The ^{1}H NMR spectrum of **T3** (Figures 7a and S23) showed six distinct peaks in the aromatic region (δ = 7.17–8.82 ppm), corroborating with the simple tubular structure as obtained from SC-XRD data (Figure 6). Furthermore, ^{1}H DOSY (Figure S24) gave a single band ($D = 1.41 \times 10^{-10}$ m^2/s) with a hydrodynamic radius of 17.4 Å (close to the nonsolvated radius of 16.3 Å obtained from the crystal structure) (Figure S57, Table S5, and Section S8). Finally, the composition of **T3** as $(\mathbf{M2})_6(\mathbf{L3})_3$ was reaffirmed from ESI-MS analyses of the PF_6^- analogue (Figures 7b,c, S25, and S26). ESI-MS displayed peaks and isotopic distributions at m/z = 1042.5726, 805.0678, and 646.7214, corresponding to the charged fragments $[\mathbf{T3}\cdot 8PF_6]^{4+}$, $[\mathbf{T3}\cdot 7PF_6]^{5+}$, and $[\mathbf{T3}\cdot 6PF_6]^{6+}$, respectively, confirming the composition of $(\mathbf{M2})_6(\mathbf{L3})_3$.

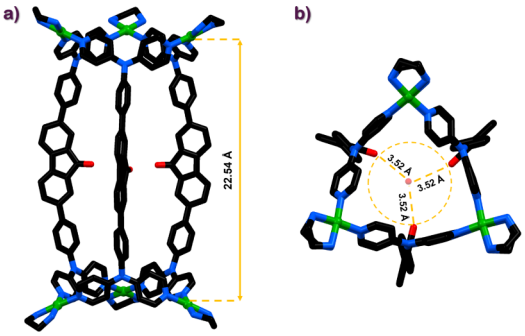

Figure 6. SC-XRD structure of **T3**: (a) side view and (b) top view. Color codes: carbon (black), nitrogen (blue), oxygen (red), and palladium (green). Solvent molecules, counter-anions, and H atoms are omitted for clarity.

The SC-XRD structure depicted that the fluorenone carbonyl groups of the ligands in **T3** pointed toward the internal cavity due to the obtuse angle (ca. 159°) subtended by the dipyridyl amine units with respect to the central core in **L3**. Thus, with the gradual angular modulation of **L1**, either by adjusting coordination vector angles (**L2**) or by extending donor ligand lengths (**L3**), it was possible to synthesize analogous tube-like architectures (**T1**, **T2**, and **T3**) with different geometries and variable-sized confined pockets (Scheme 3).

Comparative Guest Binding Abilities of the Trifacial Tubes

The controlled angular modulation affected the carbonyl group's orientation in the tubes' hydrophobic cavity (Scheme 3). This prompted us to compare the host–guest chemistry of the tubes (**T1** and **T2**). The earlier reported **T1** has three carbonyl groups from fluorenone directed into the cavity. This helped in the selective recognition of E-stilbene from a 1:1 mixture of E/Z-stilbene due to better stabilization of one E-stilbene (**G1**) molecule within its cavity, driven by strong C–H···O interactions between the alkene protons of stilbene and fluorenone's carbonyl group, forming **G1@T1** (Figure S28).[56] Further, azobenzene (**G2**) was used as an analogous guest for **T1** (Scheme 4). Adding **G2** (excess) to an aqueous solution of **T1**, followed by stirring for 12 h at room temperature, led to the formation of a turbid, bright orange solution. The solution was centrifuged, and its ^{1}H NMR spectrum was recorded (Figures 8c and S29). The ^{1}H NMR spectrum was completely desymmetrized, with guest peaks upfield-shifted, and the stoichiometry of the host–guest complex was found to be 1:1, as determined from NMR integrations (Figure S29). This corroborated with the DFT optimization studies, which showed **T1** could stabilize one **G2** molecule within its cavity via similar H-bonding interactions between the aromatic *ortho* protons of azobenzene and fluorenone's carbonyl oxygen, forming a 1:1 host–guest complex, **G2@T1** (Figure S52). Further, ^{1}H NMR titrations were carried out to verify the host–guest stoichiometries and calculate the apparent binding constants. Solutions of **T1** (in D_2O) were titrated gradually with guests **G1**/**G2** (in CD_3OD). In both cases, the host **T1** peaks showed shifts upon the addition of **G1**/**G2** and showed saturation when up to 1 equiv of the respective guests **G1**/**G2** were added, confirming the formation of 1:1 complexes, **G1@T1** and **G2@T1**, respectively. The apparent association constants (K_a) were determined to be ca. 1959 and 2463

https://doi.org/10.1021/jacsau.5c00390
JACS Au 2025, 5, 2368–2378

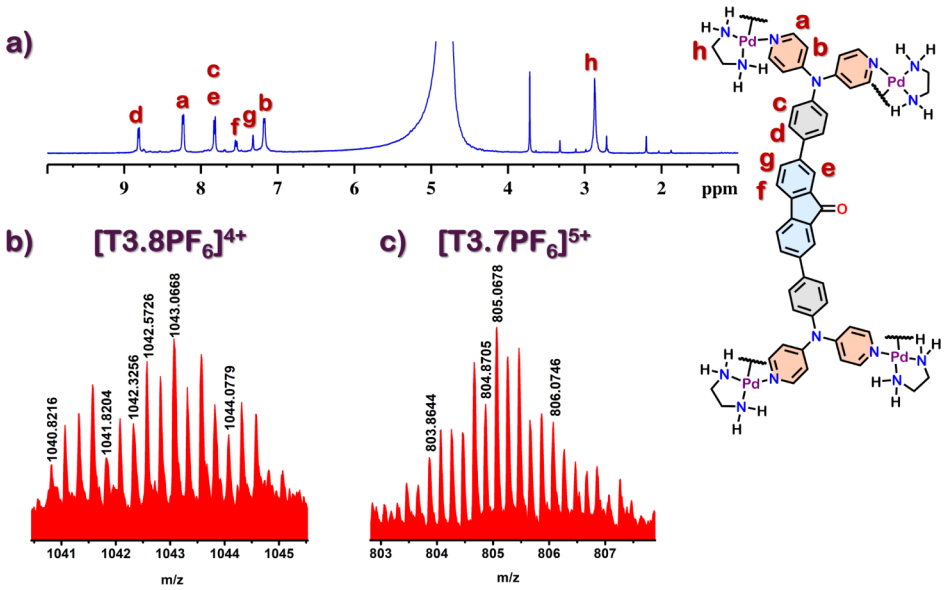

Figure 7. (a) ^{1}H NMR spectrum of **T3** recorded in D_2O. Isotopic patterns obtained in ESI-MS of the PF_6^- analogue corresponding to the charged fragments: (b) $[\mathbf{T3}\cdot 8PF_6]^{4+}$ and (c) $[\mathbf{T3}\cdot 7PF_6]^{5+}$.

Scheme 3. Schematic Representation Showing Angular Variation in Ligand (L1−L3) Leads to the Formation of Trifacial Tubes T1, T2, and T3, Respectively, of Variable Geometries and Cavity Sizes

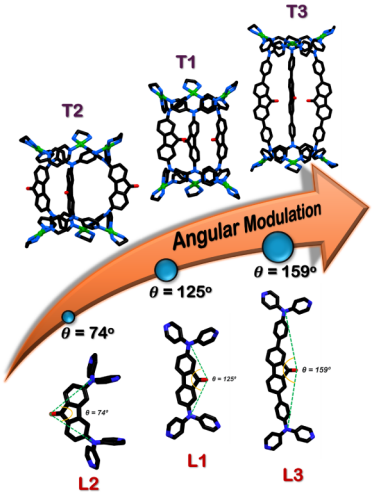

Scheme 4. Schematic Representation Shows the Encapsulation/Interaction of G1, G2, and G3 with T1 Due to the Inward Orientation of the Fluorenone Carbonyl Group within the Cavity, Whereas T2 Shows No Encapsulation of the Guests as There Are No Stabilizing Interactions Due to the Outward Orientation of Fluorenone Carbonyl Groups with Respect to the Cavity

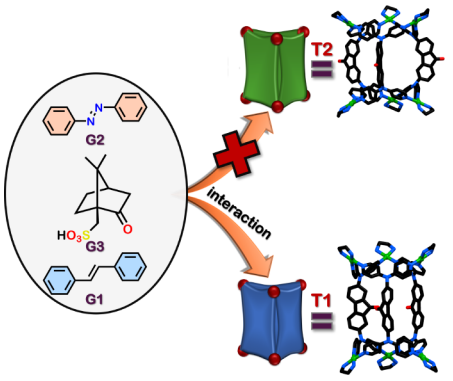

M^{-1}, respectively after fitting these titration data into Hill's equation, suggesting these complexes to be moderately stable (see Section S6, Table S2, and Figures S39−S42). However, once the orientation of the carbonyl group changes in **T2**, the ability of **T2** to encapsulate **G1**/**G2** is lost, as there are no stabilizing interactions (Figures 8d and S33).

Here, the host−guest property of the tubes is primarily governed by hydrogen bonding interactions. The guest molecules (**G1** and **G2**) explored had poor solubility in aqueous media, which ensured that the solvation of the guests did not oppose the formation of the host−guest complexes. Thus, we investigated the tendency of **T1** or **T2** to bind water-soluble guest molecules through host−guest interactions that are strong enough to overcome the solvation enthalpy of water-soluble guests. We selected a water-soluble aliphatic guest molecule, camphor sulfonic acid (**CSA**), in enantiopure form (**D-CSA**). The addition of 2 equiv of **D-CSA** (**G3**) to a D_2O solution of **T1** and stirring at room temperature for 12 h resulted in a clear solution. The ^{1}H NMR signals of **T1** became highly desymmetrized, with multifold splitting of α and β pyridyl protons due to interactions of **G3** with the protons of host **T1** (Figures 8e and S35). The **G3** peaks were upfield-shifted, indicating that **G3** interacted strongly with the cavity of **T1**. The host−guest stoichiometry was found to be 1:2 from NMR integrations, indicating the formation of the host−guest complex, $(\mathbf{G3})_2@\mathbf{T1}$. Further, ^{1}H−^{1}H NOESY showed correlations between the protons of host **T1** and guest **G3**, confirming their proximity (Figure S36). Next, we optimized the structure of $(\mathbf{G3})_2@\mathbf{T1}$ using the PM6 semi-empirical method. In the energy-optimized structure, we observed that two **G3** molecules could exactly fit inside the cavity of **T1** and are stabilized by H-bonding interactions between the inwardly oriented fluorenone oxygens of **T1** and aliphatic protons of **G3** at the center of **T1**'s cavity (Figure S53). Additionally, H-bonding interactions between aromatic protons of **T1** and the

https://doi.org/10.1021/jacsau.5c00390
JACS Au 2025, 5, 2368−2378

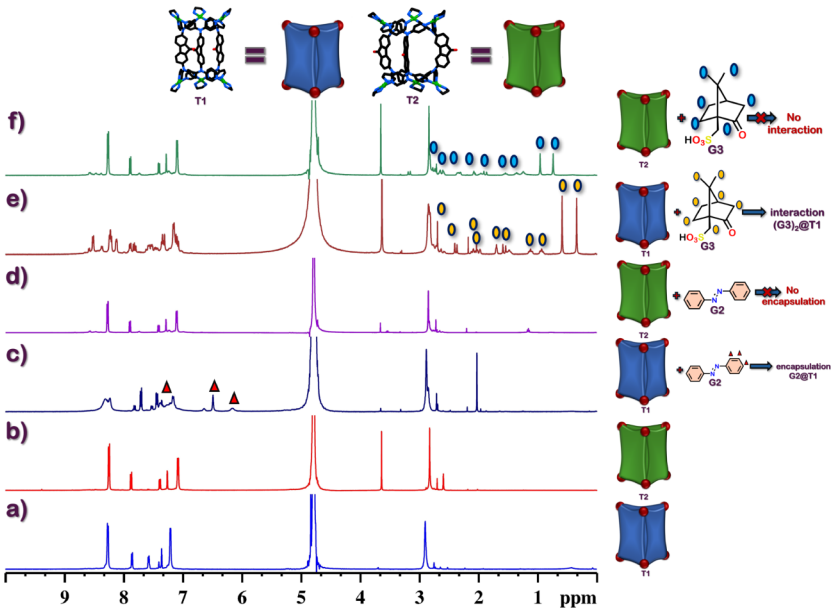

Figure 8. Stacked ^{1}H NMR displaying the variation in the host−guest properties of **T1** and **T2**. ^{1}H NMR spectra of (a) **T1**, (b) **T2**, (c) **G2@T1**, (d) after addition of excess of **G2** to **T2**, (e) $(\mathbf{G3})_2$**@T1**, and (f) after addition of 2 equiv of **G3** to **T2**. All spectra were recorded in D_2O. **T1** encapsulates **G2** and **G3,** which can be seen from the upfield shift of guest protons and desymmetrization of the host **T1**. **T2** shows no change in NMR in the presence of these guests, indicating its inability to bind guest molecules.

oxygen atoms of the sulfonic acid groups of each **G3**, located near the portals, locked two **G3** molecules within the cavity of **T1** (Figure S53). The ^{1}H NMR titrations were carried out by gradual addition of **G3** (in D_2O) to the solution of **T1** (in D_2O) which corroborated the 1:2 host−guest stoichiometry. The apparent binding constant was determined to be ca. 1021 M^{-1} (see Section S6, Table S2, and Figures S43 and S44). Next, we added 2 equiv of **G3** to an aqueous solution of **T2** and stirred the mixture at room temperature for 12 h. ^{1}H NMR displayed only peaks corresponding to free host **T2**, and unshifted free peaks of **G3** (Figures 8f and S38). This indicated that **T2** failed to bind **G3,** unlike **T1**. We optimized the probable structure of $(\mathbf{G3})_2$**@T2** by placing two **G3** molecules within the cavity of **T2** to examine the possible interactions present. The structure of $(\mathbf{G3})_2$**@T2** could only be weakly stabilized by H-bonding interactions between aromatic protons of host **T2** and the oxygen atoms of the sulfonic acid group of each **G3** at the portals (Figure S54). Finally, $(\mathbf{G3})_2$**@T1** was found to be more stable than $(\mathbf{G3})_2$**@T2** by ca. 70 kcal/mol, as observed from energy calculations (Table S4, Section S7). This again shows the importance of the orientation of certain functional groups of host molecules for binding specific guest molecules (Scheme 4).

The host−guest studies could not be carried out with **T3** as its crystals were only sparingly soluble in aqueous media, making the system less accessible for the exploration of its host−guest chemistry. An increase in the hydrophobic part (by introducing two phenyl rings within the donor ligands) hampers the water solubility of the final assembly, making it unsuitable for host−guest chemistry studies in aqueous media.

CONCLUSIONS

In conclusion, we report here the synthesis of a new molecular basket $(\mathbf{M1})_{16}(\mathbf{L1})_8$ (**B**) architecture of reduced symmetry via the self-assembly of a conformationally flexible ligand (**L1**) with a sterically demanding metal acceptor, [Pd(tmed)-$(ONO_2)_2$] (**M1**). The structure of **B** is unique in many ways. It can be described as an architecture obtained by the deformation of a symmetric Johnson polyhedron, a square orthobicupola (J_{28}), enabled by the twisting ability of donor ligands (**L1**) and the steric crowding of methyl groups (present in **M1**) near the coordination sites. At the same time, the structure is not knotted or interlocked and can be described as two distorted macrocycles sitting on top of one another, thereby demonstrating how subtle design modifications and the judicious combination of building units can yield unique and complex supramolecular architectures. Herein, we could assemble as many as 24 subcomponents into a single discrete architecture of lower symmetry, which is a challenging aspect in coordination-driven self-assembly. The selective synthesis of such entropically disfavored, complex architectures in quantitative yields exemplifies the efficiency of coordination-driven self-assembly over traditional covalent bond formation approaches. Such large, twisted, and desymmetrized architecture closely resembles natural systems and could be a model for studying functional aspects of enzymes or other biological processes.

Further, we synthesized two other fluorenone-based ligands (**L2** and **L3**), differing in their angular dispositions of ligand donor sites. Self-assembly of the ligands (**L1**, **L2**, and **L3**) with *cis*-blocked Pd(II) acceptor [Pd(en)$(ONO_2)_2$] (**M2**) results in the formation of $(\mathbf{M2})_6(\mathbf{Ln})_3$ [**Ln** = **L1**/**L2**/**L3**] trifacial tubes of similar composition but different geometries. The change in the position of the coordinating moiety, dipyridyl amine, on the fluorenone core from **L1** to **L2** led to a decrease in the angle subtended by the dipyridyl amine units to the fluorenone core. Conversely, the extension of **L1** to form an elongated analogue, **L3**, increased the angle. The ligands **L1** and **L3** had obtuse angles (with respect to the central core) of 125° and 159°, respectively, which enables the carbonyl group of fluorenone to orient inside the cavity of the resulting tubes, **T1** and **T3**. On the other hand, the acute angle of 74° in **L2** causes the carbonyl group to adopt an outward orientation in the trifacial tube **T2**. Exploration of their host−guest chemistry

https://doi.org/10.1021/jacsau.5c00390
JACS Au 2025, 5, 2368−2378

revealed that **T1** could encapsulate various guests, including E-stilbene (**G1**), E-azobenzene (**G2**), and D-camphor sulfonic acid (**G3**), due to favorable H-bonding interactions made possible by the inward orientation of the fluorenone carbonyl groups with respect to the internal cavity. Conversely, **T2**, with an outward orientation of the fluorenone carbonyls with respect to the cavity, failed to stabilize **G1**, **G2**, and **G3** due to the absence of such noncovalent interactions. This study highlights how angular variation in ligand design and orientation of functional groups can influence the properties of the hydrophobic cavity of the cage and its efficiency in molecular recognition. Here, we report a strategy that may be utilized to predesign functionalized coordination cages to stabilize desired guest molecules.

■ ASSOCIATED CONTENT

Supporting Information

The Supporting Information is available free of charge at https://pubs.acs.org/doi/10.1021/jacsau.5c00390.

Additional NMR spectra, ESI-MS, experimental details, and optimized structures (PDF)

X-ray crystallographic data for molecular basket (B) (TXT)

X-ray crystallographic data for extended trifacial tube (T3) (TXT)

■ AUTHOR INFORMATION

Corresponding Author

Partha Sarathi Mukherjee − *Department of Inorganic and Physical Chemistry, Indian Institute of Science, Bangalore 560012, India;* orcid.org/0000-0001-6891-6697; Email: psm@iisc.ac.in

Authors

Medha Aggarwal − *Department of Inorganic and Physical Chemistry, Indian Institute of Science, Bangalore 560012, India*

Ranit Banerjee − *Department of Inorganic and Physical Chemistry, Indian Institute of Science, Bangalore 560012, India*

Neal Hickey − *Department of Chemical and Pharmaceutical Sciences, University of Trieste, Trieste 34127, Italy;* orcid.org/0000-0003-1271-5719

Complete contact information is available at: https://pubs.acs.org/10.1021/jacsau.5c00390

Author Contributions

P.S.M., M.A., and R.B. devised the project and designed the experiments. M.A. mostly carried out all the experimental work. M.A. and R.B. analyzed the results. N.H. carried out the crystallographic studies in Italy. R.B. carried out the optimization studies. All the authors were involved in writing the manuscript, and they have approved the final version of the manuscript.

Notes

The authors declare no competing financial interest.

■ ACKNOWLEDGMENTS

P.S.M. thanks the SERB (New Delhi) for the research funding in the form of the J.C. Bose Fellowship and Core Research Grant. M.A. gratefully acknowledges IISc for the research fellowship. R.B. acknowledges PMRF (India) for the research fellowship and contingency grant. The authors thank the NMR facility (under the FIST program) at the IPC Department (IISc).

■ REFERENCES

(1) Caulder, D. L.; Brückner, C.; Powers, R. E.; König, S.; Parac, T. N.; Leary, J. A.; Raymond, K. N. Design, Formation and Properties of Tetrahedral M_4L_4 and M_4L_6 Supramolecular Clusters[1]. *J. Am. Chem. Soc.* **2001**, *123* (37), 8923−8938.

(2) Fujita, M.; Tominaga, M.; Hori, A.; Therrien, B. Coordination Assemblies from a Pd(II)-Cornered Square Complex. *Acc. Chem. Res.* **2005**, *38* (4), 369−378.

(3) Chakrabarty, R.; Mukherjee, P. S.; Stang, P. J. Supramolecular Coordination: Self-Assembly of Finite Two- and Three-Dimensional Ensembles. *Chem. Rev.* **2011**, *111* (11), 6810−6918.

(4) Sinha, N.; Hahn, F. E. Metallosupramolecular Architectures Obtained from Poly-N-heterocyclic Carbene Ligands. *Acc. Chem. Res.* **2017**, *50* (9), 2167−2184.

(5) Gan, M.-M.; Liu, J.-Q.; Zhang, L.; Wang, Y.-Y.; Hahn, F. E.; Han, Y.-F. Preparation and Post-Assembly Modification of Metalloupramolecular Assemblies from Poly(N-Heterocyclic Carbene) Ligands. *Chem. Rev.* **2018**, *118* (19), 9587−9641.

(6) Li, Y.; Jiang, Z.; Wang, M.; Yuan, J.; Liu, D.; Yang, X.; Chen, M.; Yan, J.; Li, X.; Wang, P. Giant, Hollow 2D Metalloarchitecture: Stepwise Self-Assembly of a Hexagonal Supramolecular Nut. *J. Am. Chem. Soc.* **2016**, *138* (31), 10041−10046.

(7) Hardy, M.; Tessarolo, J.; Holstein, J. J.; Struch, N.; Wagner, N.; Weisbarth, R.; Engeser, M.; Beck, J.; Horiuchi, S.; Clever, G. H.; Lützen, A. A Family of Heterobimetallic Cubes Shows Spin-Crossover Behaviour Near Room Temperature. *Angew. Chem., Int. Ed.* **2021**, *60* (41), 22562−22569.

(8) Zhang, Z.-E.; Zhang, Y.-F.; Zhang, Y.-Z.; Li, H.-L.; Sun, L.-Y.; Wang, L.-J.; Han, Y.-F. Construction and Hierarchical Self-Assembly of Multifunctional Coordination Cages with Triangular Metal−Metal-Bonded Units. *J. Am. Chem. Soc.* **2023**, *145* (13), 7446−7453.

(9) Bao, S.-J.; Zou, Y.; Zhang, H.-N.; Jin, G.-X. The codriven assembly of molecular metalla-links (613, 623) and metalla-knots (41, 31) via coordination and noncovalent interactions. *Proc. Natl. Acad. Sci. U. S. A.* **2024**, *121* (27), No. e2407570121.

(10) Zou, Y.; Bao, S.-J.; Tang, H.; Zhang, H.-N.; Jin, G.-X. Synergizing Steric Hindrance and Stacking Interactions To Facilitate the Controlled Assembly of Multiple 4 1 Metalla-Knots and Pseudo -Solomon Links. *Angew. Chem., Int. Ed.* **2024**, *63* (40), No. e202410722.

(11) Yan, X.; Wang, H.; Hauke, C. E.; Cook, T. R.; Wang, M.; Saha, M. L.; Zhou, Z.; Zhang, M.; Li, X.; Huang, F.; Stang, P. J. A Suite of Tetraphenylethylene-Based Discrete Organoplatinum(II) Metallacycles: Controllable Structure and Stoichiometry, Aggregation-Induced Emission, and Nitroaromatics Sensing. *J. Am. Chem. Soc.* **2015**, *137* (48), 15276−15286.

(12) Dey, S.; Aggarwal, M.; Chakraborty, D.; Mukherjee, P. S. Uncovering tetrazoles as building blocks for constructing discrete and polymeric assemblies. *Chem. Commun.* **2024**, *60* (43), 5573−5585.

(13) Sullivan, M. G.; Welgama, H. K.; Crawley, M. R.; Friedman, A. E.; Cook, T. R. Phase-Pure Zirconium Metal−Organic Polyhedra Enabled by a Ligand Substitution Strategy. *Chem. Mater.* **2024**, *36* (1), 567−574.

(14) Jin, T.; Zeng, K.; Zhang, X.; Dou, W.-T.; Hu, L.; Zhang, D.; Zhu, W.; Qian, X.; Yang, H.-B.; Xu, L. Efficient Self-Sorting Behaviours of Metallacages with Subtle Structural Differences. *Angew. Chem., Int. Ed.* **2024**, *63*, No. e202409878.

(15) McTernan, C. T.; Davies, J. A.; Nitschke, J. R. Beyond Platonic: How to Build Metal-Organic Polyhedra Capable of Binding Low-Symmetry, Information-Rich Molecular Cargoes. *Chem. Rev.* **2022**, *122* (11), 10393−10437.

(16) Yang, Y.; Ronson, T. K.; Teeuwen, P. C. P.; Du, Y.; Zheng, J.; Wales, D. J.; Nitschke, J. R. Guest binding is governed by multiple stimuli in low-symmetry metal-organic cages containing bis-pyridyl-(imine) vertices. *Chem* **2025**, *11* (1), 102288.
(17) Andrews, K. G.; Horton, P. N.; Coles, S. J. Programmable synthesis of organic cages with reduced symmetry. *Chem. Sci.* **2024**, *15* (17), 6536.
(18) Metherell, A. J.; Ward, M. D. Geometric isomerism in coordination cages based on tris-chelate vertices: a tool to control both assembly and host/guest chemistry. *Dalton Trans.* **2016**, *45* (41), 16096−16111.
(19) Baby Sainaba, A.; Venkateswarulu, M.; Bhandari, P.; Clegg, J. K.; Sarathi Mukherjee, P. Self-Assembly of an $[M_8L2_4]^{16+}$ Intertwined Cube and a Giant $[M_{12}L1_6]^{24+}$ Orthobicupola. *Angew. Chem., Int. Ed.* **2024**, *63* (1), No. e202315572.
(20) Sudan, S.; Fadaei-Tirani, F.; Severin, K. A five-stranded heterometallic helicate. *Chem. Commun.* **2023**, *59* (53), 8258−8261.
(21) Hou, Y.; Zhang, Z.; Lu, S.; Yuan, J.; Zhu, Q.; Chen, W.-P.; Ling, S.; Li, X.; Zheng, Y.-Z.; Zhu, K.; Zhang, M. Highly Emissive Perylene Diimide-Based Metallacages and Their Host−Guest Chemistry for Information Encryption. *J. Am. Chem. Soc.* **2020**, *142* (44), 18763−18768.
(22) Liu, H.; Guo, C.; Li, L.; Zhang, Z.; Hou, Y.; Mu, C.; Hou, G.; Zhang, Z.; Wang, H.; Li, X.; Zhang, M. Multicomponent, Multicavity Metallacages That Contain Different Binding Sites for Allosteric Recognition. *J. Am. Chem. Soc.* **2024**, *146* (23), 15787−15795.
(23) Xue, W.; Pesce, L.; Bellamkonda, A.; Ronson, T. K.; Wu, K.; Zhang, D.; Vanthuyne, N.; Brotin, T.; Martinez, A.; Pavan, G. M.; Nitschke, J. R. Subtle Stereochemical Effects Influence Binding and Purification Abilities of an $Fe^{II}_4L_4$ Cage. *J. Am. Chem. Soc.* **2023**, *145* (9), 5570−5577.
(24) Platzek, A.; Juber, S.; Yurtseven, C.; Hasegawa, S.; Schneider, L.; Drechsler, C.; Ebbert, K. E.; Rudolf, R.; Yan, Q.-Q.; Holstein, J. J.; Schäfer, L. V.; Clever, G. H. Endohedrally Functionalized Heteroleptic Coordination Cages for Phosphate Ester Binding. *Angew. Chem., Int. Ed.* **2022**, *61* (47), No. e202209305.
(25) Ueda, M.; Kishida, N.; Catti, L.; Yoshizawa, M. Caged bulky organic dyes in a polyaromatic framework and their spectroscopic peculiarities. *Chem. Sci.* **2022**, *13* (29), 8642−8648.
(26) Sun, G.; Zhang, X.; Zheng, Z.; Zhang, Z.-Y.; Dong, M.; Sessler, J. L.; Li, C. Chiral Macrocycles for Enantioselective Recognition. *J. Am. Chem. Soc.* **2024**, *146* (38), 26233−26242.
(27) Morozov, B. S.; Gargiulo, F.; Ghule, S.; Lee, D. J.; Hampel, F.; Kim, H. M.; Kataev, E. A. Macrocyclic Conformational Switch Coupled with Pyridinium-Induced PET for Fluorescence Detection of Adenosine Triphosphate. *J. Am. Chem. Soc.* **2024**, *146* (10), 7105−7115.
(28) Morozov, B. S.; Oshchepkov, A. S.; Klemt, I.; Agafontsev, A. M.; Krishna, S.; Hampel, F.; Xu, H.-G.; Mokhir, A.; Guldi, D.; Kataev, E. A. Supramolecular Recognition of Cytidine Phosphate in Nucleotides and RNA Sequences. *JACS Au* **2023**, *3* (3), 964−977.
(29) Han, H.; Fu, R.; Wang, R.; Tang, C.; He, M.-M.; Deng, J.-Y.; Guo, D.-S.; Stoddart, J. F.; Cai, K. Corralarenes: A Family of Conjugated Tubular Hosts. *J. Am. Chem. Soc.* **2022**, *144* (44), 20351−20362.
(30) Ding, Y.; Alimi, L. O.; Moosa, B.; Maaliki, C.; Jacquemin, J.; Huang, F.; Khashab, N. M. Selective adsorptive separation of cyclohexane over benzene using thienothiophene cages. *Chem. Sci.* **2021**, *12* (14), 5315−5318.
(31) Yan, D.-N.; Cai, L.-X.; Hu, S.-J.; Zhou, Y.-F.; Zhou, L.-P.; Sun, Q.-F. An Organo-Palladium Host Built from a Dynamic Macrocyclic Ligand: Adaptive Self-Assembly, Induced-Fit Guest Binding, and Catalysis. *Angew. Chem., Int. Ed.* **2022**, *61* (42), No. e202209879.
(32) Bierschenk, S. M.; Pan, J. Y.; Settineri, N. S.; Warzok, U.; Bergman, R. G.; Raymond, K. N.; Toste, F. D. Impact of Host Flexibility on Selectivity in a Supramolecular Host-Catalyzed Enantioselective aza-Darzens Reaction. *J. Am. Chem. Soc.* **2022**, *144* (25), 11425−11433.
(33) Takezawa, H.; Iizuka, K.; Fujita, M. Selective Synthesis and Functionalization of an Acyclic Methylene-Bridged-Arene Trimer in a Cage. *Angew. Chem., Int. Ed.* **2024**, *63* (6), No. e202319140.
(34) Boaler, P. J.; Piskorz, T. K.; Bickerton, L. E.; Wang, J.; Duarte, F.; Lloyd-Jones, G. C.; Lusby, P. J. Origins of High-Activity Cage-Catalyzed Michael Addition. *J. Am. Chem. Soc.* **2024**, *146* (28), 19317−19326.
(35) Rinshad, V. A.; Aggarwal, M.; Clegg, J. K.; Mukherjee, P. S. Harnessing a Pd_4 Water-Soluble Molecular Capsule as a Size-Selective Catalyst for Targeted Oxidation of Alkyl Aromatics. *JACS Au* **2024**, *4* (8), 3238−3247.
(36) Saha, R.; Mondal, B.; Mukherjee, P. S. Molecular Cavity for Catalysis and Formation of Metal Nanoparticles for Use in Catalysis. *Chem. Rev.* **2022**, *122* (14), 12244−12307.
(37) Zhang, D.; Ronson, T. K.; Zou, Y.-Q.; Nitschke, J. R. Metal−organic cages for molecular separations. *Nat. Rev. Chem.* **2021**, *5* (3), 168−182.
(38) Zhang, W.-Y.; Lin, Y.-J.; Han, Y.-F.; Jin, G.-X. Facile Separation of Regioisomeric Compounds by a Heteronuclear Organometallic Capsule. *J. Am. Chem. Soc.* **2016**, *138* (33), 10700−10707.
(39) Sainaba, A. B.; Venkateswarulu, M.; Bhandari, P.; Arachchige, K. S. A.; Clegg, J. K.; Mukherjee, P. S. An Adaptable Water-Soluble Molecular Boat for Selective Separation of Phenanthrene from Isomeric Anthracene. *J. Am. Chem. Soc.* **2022**, *144* (16), 7504−7513.
(40) Chakraborty, D.; Pradhan, S.; Clegg, J. K.; Mukherjee, P. S. Mechanically Interlocked Water-Soluble Pd6 Host for the Selective Separation of Coal Tar-Based Planar Aromatic Molecules. *Inorg. Chem.* **2024**, *63* (32), 14924−14932.
(41) Canton, M.; Grommet, A. B.; Pesce, L.; Gemen, J.; Li, S.; Diskin-Posner, Y.; Credi, A.; Pavan, G. M.; Andréasson, J.; Klajn, R. Improving Fatigue Resistance of Dihydropyrene by Encapsulation within a Coordination Cage. *J. Am. Chem. Soc.* **2020**, *142* (34), 14557−14565.
(42) Howlader, P.; Mondal, B.; Purba, P. C.; Zangrando, E.; Mukherjee, P. S. Self-Assembled Pd(II) Barrels as Containers for Transient Merocyanine Form and Reverse Thermochromism of Spiropyran. *J. Am. Chem. Soc.* **2018**, *140* (25), 7952−7960.
(43) Galan, A.; Ballester, P. Stabilization of reactive species by supramolecular encapsulation. *Chem. Soc. Rev.* **2016**, *45* (6), 1720−1737.
(44) Yamashina, M.; Tanaka, Y.; Lavendomme, R.; Ronson, T. K.; Pittelkow, M.; Nitschke, J. R. An antiaromatic-walled nanospace. *Nature* **2019**, *574* (7779), 511−515.
(45) Yang, Y.; Ronson, T. K.; Lu, Z.; Zheng, J.; Vanthuyne, N.; Martinez, A.; Nitschke, J. R. A curved host and second guest cooperatively inhibit the dynamic motion of corannulene. *Nat. Commun.* **2021**, *12* (1), 4079.
(46) Banerjee, R.; Chakraborty, D.; Jhang, W.-T.; Chan, Y.-T.; Mukherjee, P. S. Structural Switching of a Distorted Trigonal Metal-Organic Cage to a Tetragonal Cage and Singlet Oxygen Mediated Oxidations. *Angew. Chem., Int. Ed.* **2023**, *62* (28), No. e202305338.
(47) Chakraborty, D.; Ali, S.; Choudhury, P.; Hickey, N.; Mukherjee, P. S. Cavity-Shape-Dependent Divergent Chemical Reaction inside Aqueous Pd_6L_4 Cages. *J. Am. Chem. Soc.* **2023**, *145* (49), 26973−26982.
(48) Lewis, J. E. M. Molecular engineering of confined space in metal−organic cages. *Chem. Commun.* **2022**, *58* (100), 13873−13886.
(49) Li, R.-J.; Fadaei-Tirani, F.; Scopelliti, R.; Severin, K. Tuning the Size and Geometry of Heteroleptic Coordination Cages by Varying the Ligand Bent Angle. *Chem. —Eur. J.* **2021**, *27* (36), 9439−9445.
(50) Fujita, D.; Ueda, Y.; Sato, S.; Yokoyama, H.; Mizuno, N.; Kumasaka, T.; Fujita, M. Self-Assembly of $M_{30}L_{60}$ Icosidodecahedron. *Chem* **2016**, *1* (1), 91−101.
(51) Bloch, W. M.; Holstein, J. J.; Dittrich, B.; Hiller, W.; Clever, G. H. Hierarchical Assembly of an Interlocked M_8L_{16} Container. *Angew. Chem., Int. Ed.* **2018**, *57* (19), 5534−5538.
(52) Wu, K.; Benchimol, E.; Baksi, A.; Clever, G. H. Non-statistical assembly of multicomponent $[Pd_2ABCD]$ cages. *Nat. Chem.* **2024**, *16* (4), 584−591.

https://doi.org/10.1021/jacsau.5c00390
JACS Au 2025, 5, 2368−2378

(53) Bloch, W. M.; Abe, Y.; Holstein, J. J.; Wandtke, C. M.; Dittrich, B.; Clever, G. H. Geometric Complementarity in Assembly and Guest Recognition of a Bent Heteroleptic cis-$[Pd_2LA_2LB_2]$ Coordination Cage. *J. Am. Chem. Soc.* **2016**, *138* (41), 13750−13755.
(54) Abe, T.; Takeuchi, K.; Higashi, M.; Sato, H.; Hiraoka, S. Rational design of metal−organic cages to increase the number of components via dihedral angle control. *Nat. Commun.* **2024**, *15* (1), 7630.
(55) Banerjee, R.; Chakraborty, D.; Mukherjee, P. S. Molecular Barrels as Potential Hosts: From Synthesis to Applications. *J. Am. Chem. Soc.* **2023**, *145* (14), 7692−7711.
(56) Aggarwal, M.; Banerjee, R.; Hickey, N.; Mukherjee, P. S. Stimuli-Mediated Structural Interchange Between Pd_6 and Pd_{12} Architectures: Selective Recognition of E-Stilbene by the Pd_6 Architecture and its Photoprotection. *Angew. Chem., Int. Ed.* **2024**, *63* (50), No. e202411513.
(57) Cecot, G.; Marmier, M.; Geremia, S.; De Zorzi, R.; Vologzhanina, A. V.; Pattison, P.; Solari, E.; Tirani, F. F.; Scopelliti, R.; Severin, K. The Intricate Structural Chemistry of $M^{II}_{2n}L_n$-Type Assemblies. *J. Am. Chem. Soc.* **2017**, *139* (24), 8371−8381.
(58) Maitra, P. K.; Bhattacharyya, S.; Hickey, N.; Mukherjee, P. S. Self-Assembly of a Water-Soluble Pd_{16} Square Bicupola Architecture and Its Use in Aerobic Oxidation in Aqueous Medium. *J. Am. Chem. Soc.* **2024**, *146* (22), 15301−15308.
(59) Bhat, I. A.; Jain, R.; Siddiqui, M. M.; Saini, D. K.; Mukherjee, P. S. Water-Soluble Pd_8L_4 Self-assembled Molecular Barrel as an Aqueous Carrier for Hydrophobic Curcumin. *Inorg. Chem.* **2017**, *56* (9), 5352−5360.

https://doi.org/10.1021/jacsau.5c00390
JACS Au 2025, 5, 2368−2378